

ORIGINAL ARTICLE

Orbitofrontal Cortex Neurons Respond to Sound and Activate Primary Auditory Cortex Neurons

Daniel E. Winkowski^{1,2}, Daniel A. Nagode², Kevin J. Donaldson¹, Pingbo Yin¹, Shihab A. Shamma^{1,3}, Jonathan B. Fritz¹ and Patrick O. Kanold^{1,2}

¹Institute for Systems Research, University of Maryland, College Park, MD 20742, USA, ²Department of Biology, University of Maryland, College Park, MD 20742, USA and ³Laboratoire des Systèmes Perceptifs, École Normale Supérieure, 75005 Paris, France

Address correspondence to Patrick O. Kanold, Department of Biology, University of Maryland, 1116 Biosciences Res. Bldg., College Park, MD 20742, USA.
Email: pkanold@umd.edu

Abstract

Sensory environments change over a wide dynamic range and sensory processing can change rapidly to facilitate stable perception. While rapid changes may occur throughout the sensory processing pathway, cortical changes are believed to profoundly influence perception. Prior stimulation studies showed that orbitofrontal cortex (OFC) can modify receptive fields and sensory coding in A1, but the engagement of OFC during listening and the pathways mediating OFC influences on A1 are unknown. We show in mice that OFC neurons respond to sounds consistent with a role of OFC in audition. We then show in vitro that OFC axons are present in A1 and excite pyramidal and GABAergic cells in all layers of A1 via glutamatergic synapses. Optogenetic stimulation of OFC terminals in A1 in vivo evokes short-latency neural activity in A1 and pairing activation of OFC projections in A1 with sounds alters sound-evoked A1 responses. Together, our results identify a direct connection from OFC to A1 that can excite A1 neurons at the earliest stage of cortical processing, and thereby sculpt A1 receptive fields. These results are consistent with a role for OFC in adjusting to changing behavioral relevance of sensory inputs and modulating A1 receptive fields to enhance sound processing.

Key words: auditory cortex, mouse, orbitofrontal cortex, prefrontal cortex, top-down

Introduction

Sensory environments change over a wide dynamic range on rapid timescales providing a constant challenge to the nervous system to maintain stable perception of the world and guide behavior. It is believed that successful navigation of such challenges requires equally dynamic adjustments to cortical processing. Indeed, recent electrophysiological studies in ferrets have demonstrated a capacity of neurons in primary auditory cortex (A1) to alter their response properties during behavior (Fritz et al. 2003; David et al. 2012). Moreover, A1 neurons in mice trained on a foraging task demonstrate improved decoding of relevant, training sounds with low signal-to-noise ratio as compared with other, irrelevant sounds (Whitton et al. 2014).

Thus, A1 responses and dynamics can change in complex ways to keep pace with changing environmental demands on a moment-by-moment basis.

A body of evidence has emerged pointing to higher order cortical areas as sources for dynamic changes in sensory cortices. For example, neurons in the ferret frontal cortex can signal target stimuli during behavior with high fidelity either by increasing or decreasing their activity on a given trial (Fritz et al. 2010). In mice, we recently identified the orbitofrontal cortex (OFC), a region within the prefrontal cortex, as a higher order cortical area that can rapidly adjust A1 receptive fields when tones are paired with electrical stimulation of the OFC (Winkowski et al. 2013). Using an information theoretic analysis of populations of

A1 neurons, this OFC-driven response adjustment also leads to improved neural discrimination performance of the paired tone (Winkowski et al. 2013). However, whether the OFC is activated by auditory stimuli and how OFC engages A1 remained unclear. Recently, direct influence of motor cortex on auditory evoked activity has been demonstrated, providing a synaptic and circuit basis for the audio-motor interactions (Schneider et al. 2014). Similarly, direct circuits underlying the effects of mouse motor cortex on primary somatosensory (S1) fields as well as frontal eye/orienting fields on primary visual (V1) cortical processing have been elucidated (Mao et al. 2011; Zhang et al. 2014, 2016). Given the influence of OFC stimulation on A1 (Winkowski et al. 2013), we thus investigated whether the OFC is activated by auditory stimuli and also directly interacts with circuits in A1.

Using *in vivo* recordings, we show that OFC neurons respond to auditory stimuli establishing that OFC neurons can be involved in auditory processing tasks. We then demonstrate that in mouse, there exists a direct connection between OFC and A1 and that *in vivo* optogenetic stimulation of the OFC terminals in A1 evokes short-latency neural activity in A1. Whole-cell patch-clamp recordings *in vitro* showed that OFC axons excite pyramidal and GABAergic cells in all layers of A1 via glutamatergic synapses. We then show that direct optogenetic activation of the OFC terminals in A1 can modulate A1 responses. Together, our results demonstrate a direct connection from OFC to A1 that excites A1 neurons at the earliest stage of cortical processing, and thereby has the ability to sculpt their receptive fields and improve sound processing.

Materials and Methods

All procedures were approved by the University of Maryland Institutional Animal Care and Use Committee. We used mice of either sex (6–28 weeks, C57/Bl6 or CBA strain 12–28 weeks). Wild-type (C57BL/6J, stock #00664), CBA, or transgenic mice (Ai9, JAX stock #7909; Gad2-IRES-Cre, JAX stock #10802) were originally obtained from The Jackson Laboratory and bred in house.

OFC Virus Injection

Mice were anesthetized with isoflurane and placed on a regulated thermal blanket to maintain a core temperature of 37.5 °C. The eyes were covered with a layer of ophthalmic ointment. A midline incision was made in the scalp and the dorsal surface of the skull was cleaned. The injection system consisted of a pulled glass pipette beveled at a 45-degree angle (25–30 μm outer diameter), backfilled with mineral oil and coupled to a Nanoject II microinjector (Drummond Scientific). The injection pipette was inserted into the brain under control of a Sutter manipulator (MP-285; Sutter Instruments). For physiology (*in vitro* and *in vivo*) and anterograde labeling of OFC axons, AAV2/1-CaMKIIa-hChr2(H134R)-EYFP (AAV-Chr2; 350–500 nL, UNC Vector Core, titer 2×10^{12} gc/mL) was injected into the OFC (2.5 mm rostral from bregma, 1 mm lateral from the midline (ML), 1.6 mm beneath the dorsal surface pia). For *in vitro* physiology and anatomical studies, we used mice that were the progeny of crossing Gad2-IRES-Cre with Ai9 mouse lines so that Gad2 positive (i.e. inhibitory) neurons were visible. For *in vivo* physiology, C57BL/6J were used. The minimum survival time for all injections was 2 weeks.

Optogenetic Activation of OFC Axons *In Vivo*

For electrophysiology, animals were prepared as detailed below. OFC afferents were activated using a 473-nm laser (BL473T8-150, Shanghai Laser) coupled to a 200-μm fiber positioned over A1. Light levels at the surface of the cortex were below approximately 140 mW/mm². In a subset of experiments, we infused a mixture of gamma-aminobutyric acid (GABA) agonists (5 μg/μL muscimol and 2 μg/μL baclofen in artificial CSF [ACSF]; Sigma) into the OFC on the day of the experiment to prevent antidromic activation of OFC soma during illumination of OFC axons in A1.

In Vivo Electrophysiology

Anesthetized A1 Recordings

We used C57/Bl6 mice (6–14 weeks, mean age 11.5 weeks) for recordings in A1. A 16-channel silicon probe (linear array, 177 μm² contact area, 50 μm contact separation; NeuroNexus Technologies) was used to record local field potential (LFP) activity across the different layers of A1. The linear array was slowly advanced into A1 orthogonal to the surface of the brain and electrodes were allowed to settle for more than approximately 20 min before the experiment commenced. Wide-band neural signals (0.7 Hz–8 kHz) were passed through a preamplifier (Plexon), digitized at 50 kHz, acquired with Ephus (Suter et al. 2010), and stored for offline analysis using custom software written in Matlab (Mathworks).

To analyze the LFP signals in A1, we first removed 60 Hz line noise and its second harmonic (120 Hz) from the recording using the `rmlinesc` function in Matlab, available from the Chronux toolbox (<http://www.chronux.org>). The denoised data were then low-pass filtered at 300 Hz and down-sampled to 1 kHz using the `resample` function in Matlab. Responsive channels (sites) were defined by t-test ($P < 0.01$) across all baseline (100 ms prestimulus) and all poststimulus sound presentation periods (100 ms). This criterion is somewhat conservative given that some sound stimuli do not elicit an LFP response. Nonetheless, neural signals from all responsive channels were subjected to further analysis. The peak-to-peak amplitude of the sound-evoked LFP signal (5–35 ms after sound onset [Otazu et al. 2009]) was used to determine response strength and selectivity (i.e. tuning) of each recording contact on the linear array. To quantify differences in response amplitude and tuning before and after optical OFC pairing, we computed the difference in tuning curves for each recording contact. To compare across experiments and account for any differences in baseline and/or evoked activity, the effect of OFC pairing on each recording contact was compared using a modulation index $[(\text{post} - \text{pre})/(\text{post} + \text{pre})]$. To compare across laminar groupings, the channel map was used to divide recording sites into roughly 3 equal groups based on the current source density (CSD) profile (L2/3: Channels 1–5, approximately 200 μm; L4: Channels 6–10, approximately 200 μm; and L5/6: Channels 11–16, approximately 250 μm) and the OFC pairing induced effects were then compared across groups.

For measuring sound-evoked activity in A1, sound stimuli (SAM tones, 4–64 kHz, 0.5 octave spacing, approximately 60 dB sound pressure level (SPL), duration: 400 ms, 5 Hz full-depth modulation, 4–5 s ISI, or broadband noise bursts, duration: 50 ms, 5 ms linear on and off ramps) were generated using custom software written in Matlab (Mathworks) and passed through an RX6 MultiFunction Processor for digital to analog conversion, attenuated using a PA5 and delivered through a calibrated free field speaker (Tucker-Davis Technologies ES1, driven with TDT ED1 drivers).

Awake OFC Recordings

A total of 20 mice were used, CBA ($n = 16$, 12–28 weeks, mean age 18 weeks) and C57/Bl6 ($n = 4$, 18–28 weeks). All mice were obtained from Jackson Laboratory. Mice were implanted with a small custom-made headpost (0.5 g). To preserve identification of stereotaxic landmarks, the front edge of the headpost was aligned to Bregma and centered along the midline of the skull. A flexible, U-shaped well (with a wall height of 1.5 mm) was fabricated using a custom 3D printer using ABS plastic and positioned in front of the headpost (for a saline well during recordings). Wound margins were sealed with tissue adhesive (3M Vetbond). Meloxicam (Bimeda Inc., dosage 1 mg/kg) was administered subcutaneously for analgesic and anti-inflammatory treatment. After 2–3 days of recovery from headpost implant surgery, animals began habituation to head-fixed restraint. In order to enhance adjustment to holder fixation, animals were given water reward while in the holder. Mice were placed on a water restriction schedule with daily access to water during daily holder training sessions. During these training sessions, animals received 0.3–1.0 mL of water. During the 1–2 weeks of habituation, sessions were gradually increased in duration over successive days from 15 min up to 60–90 min. Following a delay of at least 1 h posttraining, if needed, animals were given supplementary water until a total daily maximum of 1.0 mL was consumed. In addition to skin turgor testing, animal weights were measured daily prior to each training session to ensure that weights were maintained above 75% of pretraining starting weight (measured under conditions of ad libitum water).

After 1–2 weeks of habituation training, on the day prior to the first neurophysiological recording session, mice received a frontal craniotomy to permit neurophysiological recording in OFC. Animals were anesthetized with a ½ dose of ketamine/xylazine (50 mg/kg ketamine, 5 mg/kg xylazine) and a craniotomy was made directly above the intended recording location (2.5 mm anterior to Bregma, 1.0 mm ML). Recordings were conducted using either tungsten microelectrodes (2–6 M Ω , Fredrick Haer Company) or silicon linear arrays (Neuronexus 100 μ m contact separation). Electrodes were slowly inserted into the brain at the beginning of each recording session and advanced in small steps to the OFC. A custom, 32-channel recording system was constructed to acquire (National Instruments, NI PCIe-6353) and amplify (Plexon, PBX 3–64/wb-G1000) raw neural data. Multiunit (300–7000 Hz) and LFP (0.1–300 Hz) responses were monitored during recording sessions and stored for later analysis using the MANTA recording software package (Englitz et al. 2013).

To characterize auditory responses in OFC, we used a range of acoustic stimuli consisting of tone pips, frequency modulated sweeps, white and broadband noise, and rippled broadband noise (Temporally Orthogonal Ripple Combinations or TORCs). Stimuli were presented in blocks of 100 repetitions for each stimulus type, with blocks occurring in random order. Sounds were generated by custom software (Baphy, NSL), amplified (Marantz PM8010), and delivered via a calibrated ultrasonic speaker (Vifa speaker, Avisoft BioAcoustics or Fostex FT28D) inside a sound isolation booth (single wall Industrial Acoustics Company booth). Except for a few cases, stimuli were presented at 60 dB SPL and with a duration of 500 ms. Tone stimuli over 3–6 octaves (in the range 1–64 kHz) were presented in randomized frequency order with 1/5 octave spacing between tones. Bandpassed noise (BPN, 2 octaves wide) was also presented to the animals with center frequency at 20 kHz (i.e. bandpassed from 10 to 40 kHz). TORCs covered a frequency range of 2–64 kHz.

At the end of some recording sessions, electrolytic lesions were made by passing constant current (5 μ A, 2 min) at the electrode tip with an Iontophoresis Pump (Kation Scientific, Model BAB-500). The lesions marked the final recording site in each hemisphere in each animal for histological verification. The mice were then deeply anesthetized, perfused with saline and then 4% paraformaldehyde in buffered solution, and the fixed brains were removed. The brains were placed in 30% sucrose until they sank, and then cut in 50 μ M sections on a freezing microtome (Leica 2000 R). Alternate sections were stained with cresyl violet for Nissl bodies. Bright field images of tissue sections were photographed using NeuroLucida software (NeuroLucida; MicroBrightfield) connected to a microscope (Olympus BX60) that was used to image both bright field and fluorescent sections.

Single-units were isolated offline from the stored raw neural activity traces by customized spike-sorting software, which was based on a PCA and template-matching algorithm (MESKA-PCA/QuickSort, NSL). The auditory responsiveness of isolated single-units was assessed by the activity evoked by different acoustic stimuli (usually 500 ms, but ranging from 100 to 3000 ms in duration in some cases to explore the effect of sound duration on responses). To determine whether individual neurons were driven by sound stimuli, the overall poststimulus time histograms (PSTHs) with 50-ms time bins were plotted from all trials for each of the sound categories. A paired sample t-test was performed across all bins (total 10 bins) against the baseline (estimated from the 50-ms bin before stimulus onset). If any bin showed a P value less than 0.005 (Bonferroni correction for multiple measures), or if 2 consecutive bins showed a P value less than 0.05, the neuron was marked as responsive to that sound category. The rasters and PSTHs of these neurons were further inspected visually to confirm, or reject, the response, based on response consistency across trials. In order to calculate the response latency, the neural response density function was derived from the identified auditory responsive neurons, by calculating a moving average of the spiking activity across the stimulus with a 50-ms time window and 1-ms moving step. The longest rising (or falling if an inhibitory response) ramp was determined from the density functions, and the time showing the fastest slope of the ramp was marked as response latency (usually at the half height of the ramp). In a similar fashion, the peak response and peak latency were also computed from the density functions. The response from each of recording sites was also assessed by the evoked LFPs to different sound categories. The raw LFP signals were down-sampled (1000 Hz), notch filtered (60 Hz), bandpass filtered (0.5–300 Hz), and baseline corrected (averaged level of 200 ms period before stimulus onset). The overall LFPs were averaged from all traces from each of the sound categories. A one-sample t-test was performed across each sample of the overall LFP during the sound duration testing the null hypothesis that the sample came from a distribution with mean zero (i.e. no evoked LFP response). If there were more than 10 consecutive samples with a P value less than 0.05, the LFPs were marked and then further inspected visually to confirm or reject the response.

In Vitro Electrophysiology

We used C57/Bl6 for in vitro recordings. In total, 350–500 nL of AAV-ChR2 (titer 2×10^{12} gc/mL) were stereotactically injected into OFC (Paxinos and Franklin 2013). After a survival time of >2 weeks, thalamocortical (TC) brain slices were prepared in a similar procedure to prior studies from our laboratory

(Zhao et al. 2009) with the only difference being a slightly shallower slicing angle. Mice that had been injected with AAV-ChR2 construct were deeply anesthetized with isoflurane prior to decapitation and removal of the brain. Acute TC slices (500–600 μm slices from wild-type mice; 400 μm slices from Gad2 reporter mice [bred by crossing Gad2-IRES-Cre and Ai9 reporter mice] to facilitate visualization of inhibitory neurons) were prepared using a vibrating microtome (Leica) in ice-cold artificial cerebral spinal fluid (ACSF). The ACSF consisted of (in mM): 130 NaCl, 3 KCl, 1.25 NaH_2PO_4 , 20 NaHCO_3 , 10 glucose, 1.3 MgSO_4 , 2.5 CaCl, pH 7.35–7.4, equilibrated with 95% O_2 –5% CO_2 . The slices were incubated in ACSF for 1 h at 30 $^\circ\text{C}$ and then kept at room temperature. Whole-cell recordings were performed with a patch-clamp amplifier (Multiclamp 700B; Molecular Devices), digitized with a 16-bit A/D board (National Instruments), and acquired with Ephus (Suter et al. 2010). Electrodes were filled with a solution consisting of: 115 mM cesium methanesulfonate (CsCH_3SO_3), 5 mM NaF, 10 mM ethyleneglycol-bis(2-aminoethyl ether)-N,N,N',N'-tetra acetic acid, 15 mM CsCl, 3.5 mM MgATP, 3 mM QX-314, 0.5% Biocytin, pH 7.25, approximately 300 mOsm. Slices were perfused with ACSF at a rate of approximately 1 mL/min. The electrode resistance in the bath was 3–7 M Ω . OFC afferents were activated using a 470 nm light emitting diode (Thorlabs) coupled to the epifluorescence path of the microscope (Nikon FN1). Light levels at the surface of the slice approximately 5 mW delivered through either a $\times 16$ or $\times 40$ water-immersion objective. “Drugs”: 2,3-dihydroxy-6-nitro-7-sulfamoyl-benzo[f]quinoxaline-2,3-dione (NBQX, 10 μM) and D-AP5 (50 μM) were used to block α -amino-3-hydroxy-5-methyl-4-isoxazolepropionic acid and N-methyl-D-aspartate currents, respectively. 4-Aminopyridine (4-AP, 10–20 μM) was added to some slices to enhance activation of axon terminals by ChR2 stimulation.

Immunohistochemistry

C57/Bl6 mice were transcardially perfused with 0.1 M PBS followed by approximately 10 mL of fixative (4% paraformaldehyde in 0.1 M phosphate buffered saline [PBS], pH 7.4). The brain was removed and postfixed overnight at 4 $^\circ\text{C}$. Brains were equilibrated in 30% sucrose. Tissue was blocked either in the coronal plane or at approximately 15 degree angle from horizontal. The modified horizontal plane was used for improved landmark identification of the location of A1 and to roughly preserve the tonotopic frequency map (within a given slice). Brains were sectioned (50 μm thickness) on a freezing microtome and stored in 0.1 M PBS.

For immunostaining, primary antibodies used were chicken anti-GFP (1:1000; Aves, GFP-1010), mouse anti-RFP (1:500; Rockland, 200-301-379 S), and rabbit anti-parvalbumin (1:100; EMD Millipore, AB15736). Secondary antibodies used were anti-chicken Alexa488 (1:500; Life Technologies, A-11031), anti-mouse Alexa568 (1:500; Life Technologies, A-11039), and anti-rabbit DyLight488 (1:500; Vector Laboratories, DI-1488). Relevant brain sections were blocked in a solution containing 3% bovine serum and 0.3% triton in 0.1 M PBS for 1–2 h. Sections were then incubated with primary antibodies in blocking solution overnight at 4 $^\circ\text{C}$ on a shaker. The next day, the tissue was rinsed 3 times in 0.3% Triton X-100 in 0.1 M PBS and then with the appropriate secondary antibody diluted in blocking solution for 2 h at room temperature. Sections were mounted onto SuperFrost Plus slides and allowed to air dry. Dried sections were coverslipped with 4',6-diamidino-2-phenylindole (DAPI) Fluoromount-G (SouthernBiotech) and allowed to dry before image acquisition. Images were acquired in the UMD

Imaging Core using a Leica SP5X confocal microscope using $\times 10$, $\times 20$, or $\times 40$ objectives. Images were processed using ImageJ (NIH).

Results

OFC Neurons Respond to Sounds

OFC stimulation can reshape A1 receptive fields (Winkowski et al. 2013) and earlier studies on medial frontal cortex (Yang et al. 2007) suggested a role for frontal cortex in enhancing and mediating sensory receptive field plasticity. To mediate such a function, we conjectured that OFC neurons might respond to auditory stimuli. We thus investigated directly the responses of OFC to auditory stimuli. We placed electrodes into the OFC and recorded extracellular activity during sound stimulation. Since activity in frontal areas is likely to be reduced by anesthesia, we performed these experiments in awake animals. The primary target for our neurophysiological recordings was the lateral/ventral orbitofrontal (LO/VO) region, where stimulation can alter A1 receptive fields (Winkowski et al. 2013). In order to access this deep cortical area, we made perpendicular electrode penetrations into the dorsal frontal brain surface, within a defined penetration zone, located directly above LO/VO. As these electrode penetrations passed through other, more superficial and intermediate cortical areas—including M2 (premotor) and FrA (frontal association cortex), we also sparsely sampled responses in these areas as well (Fig. 1A).

We made a total of 55 electrode penetrations in frontal cortices of 20 mice, and recorded from a total of 187 sites across these penetrations (on average, approximately 2–3 penetrations per animal, and approximately 2–3 recording sites per penetration). We recorded from 244 single-units (195 in LO/VO and 49 in M2/FrA) that were isolated from 187 recording sites. Of note, 57/244 (ca. 23%) neurons were auditory responsive (42/195 (~21%) in LO/VO and 15/49 (~31%) in M2/FrA) and showed auditory response to at least one of the sound categories tested (see Methods). The vast majority (47/57 (ca. 82%) total—of which 34/42 (ca. 81%) were in LO/VO and 13/15 (ca. 87%) in M2/FrA) showed excitatory responses, while a few units showed inhibitory responses (6 neurons—all in LO/VO). There were also 4 “mixed” units (2 in LO/VO and 2 in M2/FrA) that showed excitatory response to one sound category and inhibitory response to another sound category.

The time course and amplitude of auditory responses in frontal cortex were diverse. Figure 1B–D shows 7 example neurons in frontal cortex (5 from LO/VO—Figs. 1B,C and 2 from M2—Fig. 1D). In each subpanel, the accompanying LFP responses from the same recording site are also displayed. Some cells showed short-latency onset responses, as early as 30–40 ms, and rapid monophasic peaks (as early as 50 ms) (Fig. 1B1), other cells showed a delayed, longer latency monophasic peak (at about 100 ms) followed by suppression (Fig. 1B2) or a second peak (Fig. 1D1). Some cells showed a gradual ramping to a single peak (Fig. 1B3). We also observed sustained excitatory responses in some frontal cells that could last for hundreds of millisecond (Fig. 1B3,C1). While the response onset could be time locked to stimulus onset in some cases (Fig. 1B1), usually we observed considerable latency “jitter” or stochastic variability in response onset times (Fig. 1B–D). On the whole, we found non-selective frontal responses to sound, and with a few exceptions (Fig. 1C2), cells tended to have similar responses to all acoustic stimuli presented independent of stimulus type or duration (Fig. 1B–D).

LFP responses evoked by auditory stimuli were found throughout LO/VO and M2/FrA, and often were recorded

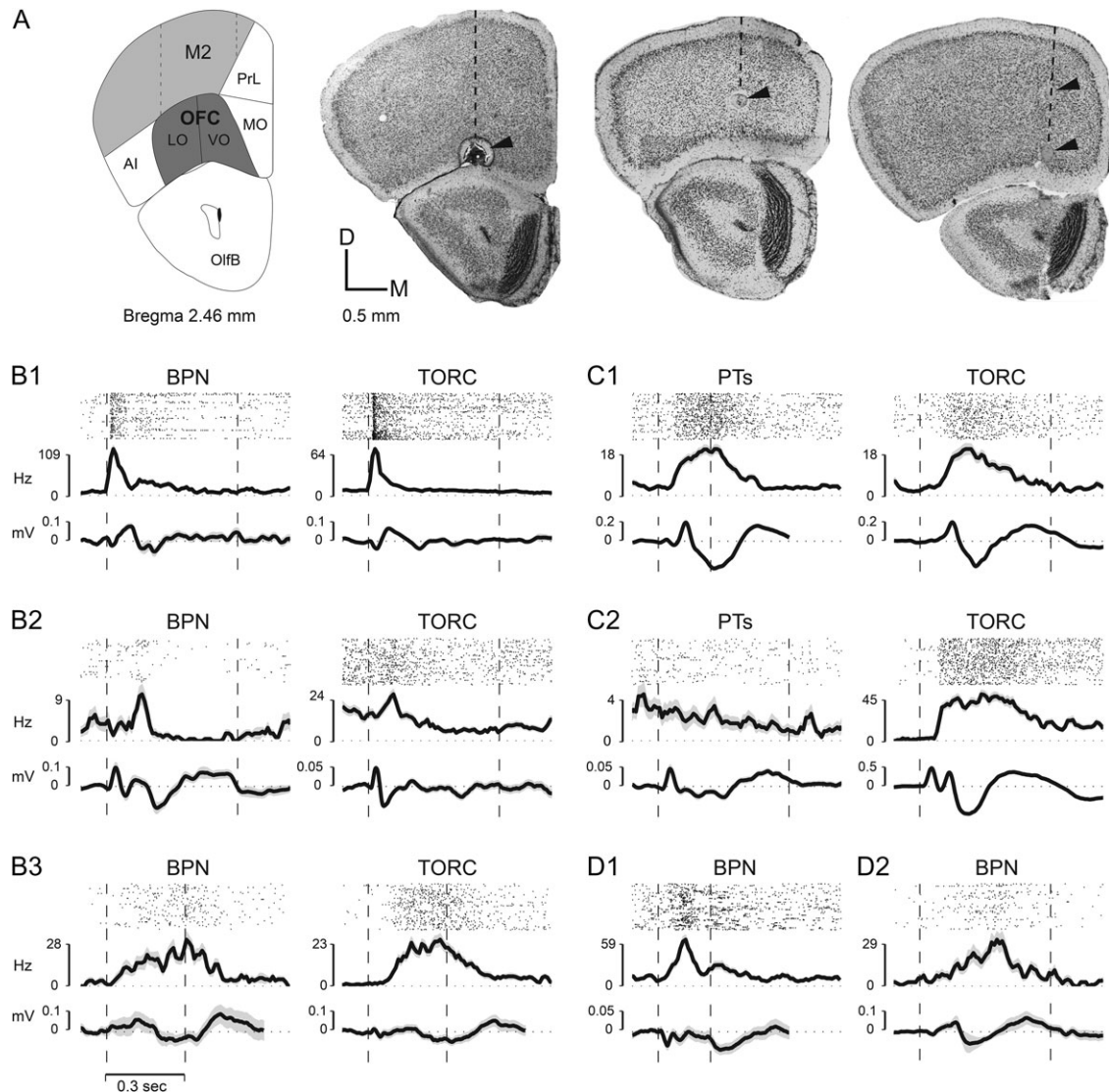


Figure 1. Single-units in OFC respond to sound. (A) Recording sites in OFC in LO and VO OFC. Top-left panel—coronal brain section (modified from Paxinos and Franklin 2013) from 2.46 mm anterior to bregma showing the position of LO/VO, lying ventral to M2 in this section (and below FrA in more anterior sections [not shown]). The adjacent 3 panels (in Fig. 1A) are coronal frontal cortex slices that illustrate the location of small electrolytic lesions placed near sites in LO/VO in 3 different mice where auditory responses were recorded. The dashed line in each brain section indicates the location of one electrode penetration, and the arrows point to the lesions made along that penetration. Each coronal section was cut at 50 μ m thickness and stained with cresyl violet for Nissl bodies. (B) Three examples of single-unit raster plots, PSTHs and site-associated LFP responses in LO/VO to broadband noise stimuli (BPN) and TORCs (B1, B2, B3). The dashed vertical lines indicate stimulus onset and offset times. Note similar responses to both types of noise stimuli. (C) Two examples (C1, C2) of single-unit PSTH and site-associated LFP responses in LO/VO to pure tones (PT) and TORCs in LO/VO neurons. Note the strong excitatory response to broadband stimuli, and lack of response to tones shown in C2. (D) Two examples (D1, D2) of single-unit PSTH and site-associated LFP responses to BPN in M2 neurons. Acoustic stimuli used include tone stimuli (100–500 ms) that ranged over 3–6 octaves with 1/5 octave spacing between tones (in the range 1–64 kHz) and were presented in randomized frequency order. BPN (100–500 ms, 2 octaves wide, i.e. 10–40 kHz) and TORCs (300 ms–3 s, 2–64 kHz) were also presented. Overall, we found non-selective OFC responses to sound, and with a few exceptions (C2), individual cells tended to have similar responses to all acoustic stimuli presented irrespective of stimulus type or duration (ranging from 200 ms [C1 PT, D1 BPN] to 1000 ms [C2 TORC]).

at sites where single-units were not responsive to auditory stimuli. More than half of the recording sites (103/187 = 55%) showed an evoked response to at least one of the sounds categories. Examples of LFP responses are shown in the lower trace of each panel in Fig. 1B–D. The LFPs generally mirrored the time course of the single-unit response dynamics from the same site, although occasionally they preceded single-unit activity (this was true of the 2 cases from M2 shown in Fig. 1D).

To identify the overall response pattern, we computed the population average of single-unit responses to 2 broadband

stimulus classes in LO/VO (Fig. 2A,B) and in M2/FrA (Fig. 2C). As shown by the boxplots in each panel, although there was considerable variability in the onset latency of auditory responses in different cells and at different sites, the overall pattern of the single-unit population response was quite similar for TORCs and BPNs (Fig. 2A–C). The average single-unit PSTH shows a response time courses with slow rising slope, arising from pooling a range of differing response latencies among the neuron population (indicated by the boxplot). The overall averaged population LFP pattern in LO/VO was also quite similar for the 2 broadband stimulus classes (Fig. 2D–F). Together, these

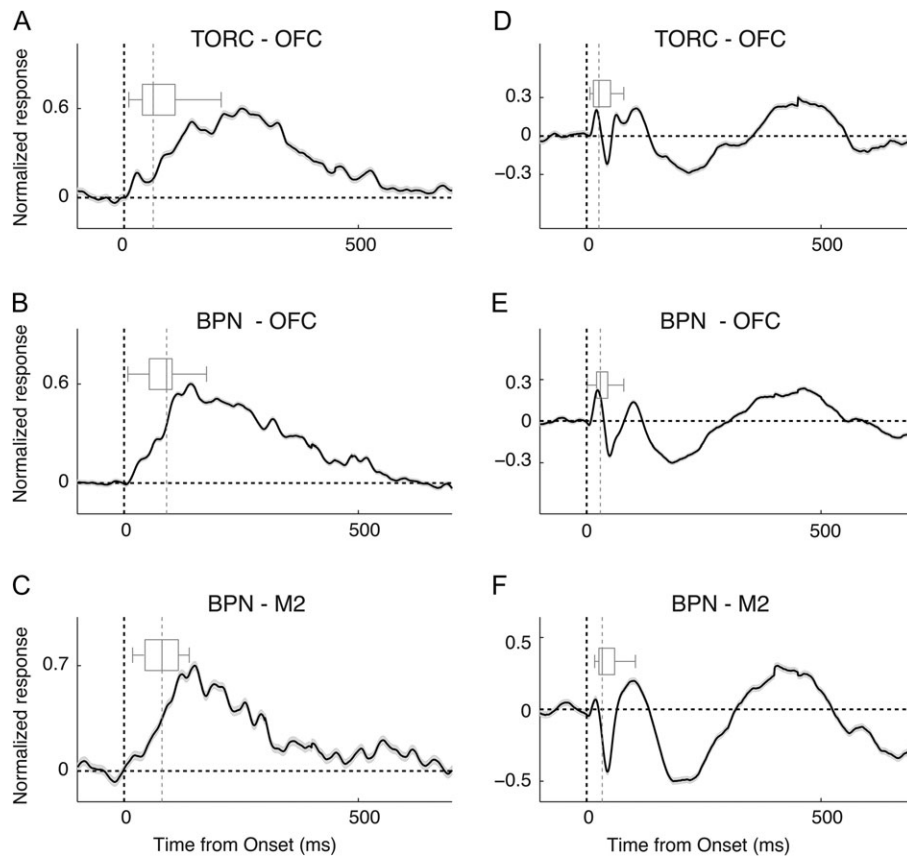


Figure 2 Average population responses to sound stimulation. Population average of single-unit PSTHs (A–C) and LFP (D–F) responses. (A,D) Averaged single-unit/LFP responses to TORCs in LO/VO neurons; (B,E) averaged single-unit/LFP responses to BPN in LO/VO neurons; (C,F) averaged single-unit/LFP responses to BPN in M2/FrA neurons. The boxplot in each panel indicates the distribution of response latency. The dashed vertical lines indicate stimulus onset (black) and median latencies (gray).

results show that a substantial fraction of OFC inputs and neurons are activated by acoustic stimuli.

Optogenetic Activation of OFC Projections to A1 In Vivo Evokes Activity in Infragranular and Supragranular Layers of A1

Our prior stimulation experiments showed that electrical stimulation of OFC could alter A1 receptive fields (Winkowski et al. 2013). However, while our prior results suggested a direct connection from OFC to A1, electrical stimulation can potentially activate multiple pathways. While there is a small but significant projection of OFC to A1 in gerbils (Budinger et al. 2008), we here aimed to test if such a projection is present in mice and if activating the OFC–A1 projection influence A1 neurons. To selectively activate OFC projections to A1, we used an optogenetic approach, injecting AAV2-ChR2-YFP into OFC and then illuminating the OFC terminals by targeting light to A1. We first confirmed that OFC in mice projects to A1 anatomically. We cut TC slices of A1 and observed YFP labeled fibers in all layers of A1 ($n = 4$ mice) (Fig. 3A). The density of YFP labeled fibers was greatest in supragranular and infragranular layers of A1 (Fig. 3A). Thus, OFC in mouse projects to A1, consistent with earlier findings in the gerbil (Budinger et al. 2008). We next investigated if selectively activating this projection by light stimulation can lead to functional responses in A1 in vivo and if so, which cortical layer is activated by the OFC–A1 projection. We injected AAV2-ChR2-YFP

into OFC and after a survival time of several weeks inserted a linear 16-channel electrode array into A1 that allowed us to record responses throughout the entire depth of A1 ($N = 7$ mice, Fig. 3B–F). We presented acoustic stimuli and performed a CSD analysis (Mitzdorf and Singer 1978). Auditory stimulation produced shortest latency event-related potentials (ERPs) and current sinks in electrodes located in midcortical layers 3b/4 (Fig. 3B,C,F) consistent with the recording location being in A1. At the same recording locations, we then optogenetically activated OFC axons in A1 by illuminating the recording location in A1 with blue light (470 nm). We found that brief (5 ms) pulses of light produced robust ERPs in A1 (Fig. 3D). CSD analysis of the light-evoked responses revealed a spatial pattern that exhibited current sinks in superficial (L1) and deeper laminae (deep L4 and below, Fig. 3E, F). The weak or absent activation in the deepest layers (i.e. L5/6) despite somewhat dense axonal innervation could be due to light scatter and failure to sufficiently and synchronously activate OFC axons at those depths. Across the population, similar patterns were observed at each recording location ($n = 7$ animals, Fig. 3F). Together, these results indicate that OFC projects directly to A1 and causes activation of multiple A1 laminae.

OFC Provides Excitation to A1 Neurons

Our experiments above establish that OFC areas project to A1, and reveal a broad projection to multiple laminae. However, dendrites of A1 neurons can extend into laminae other than that of their soma thus the OFC projections can potentially

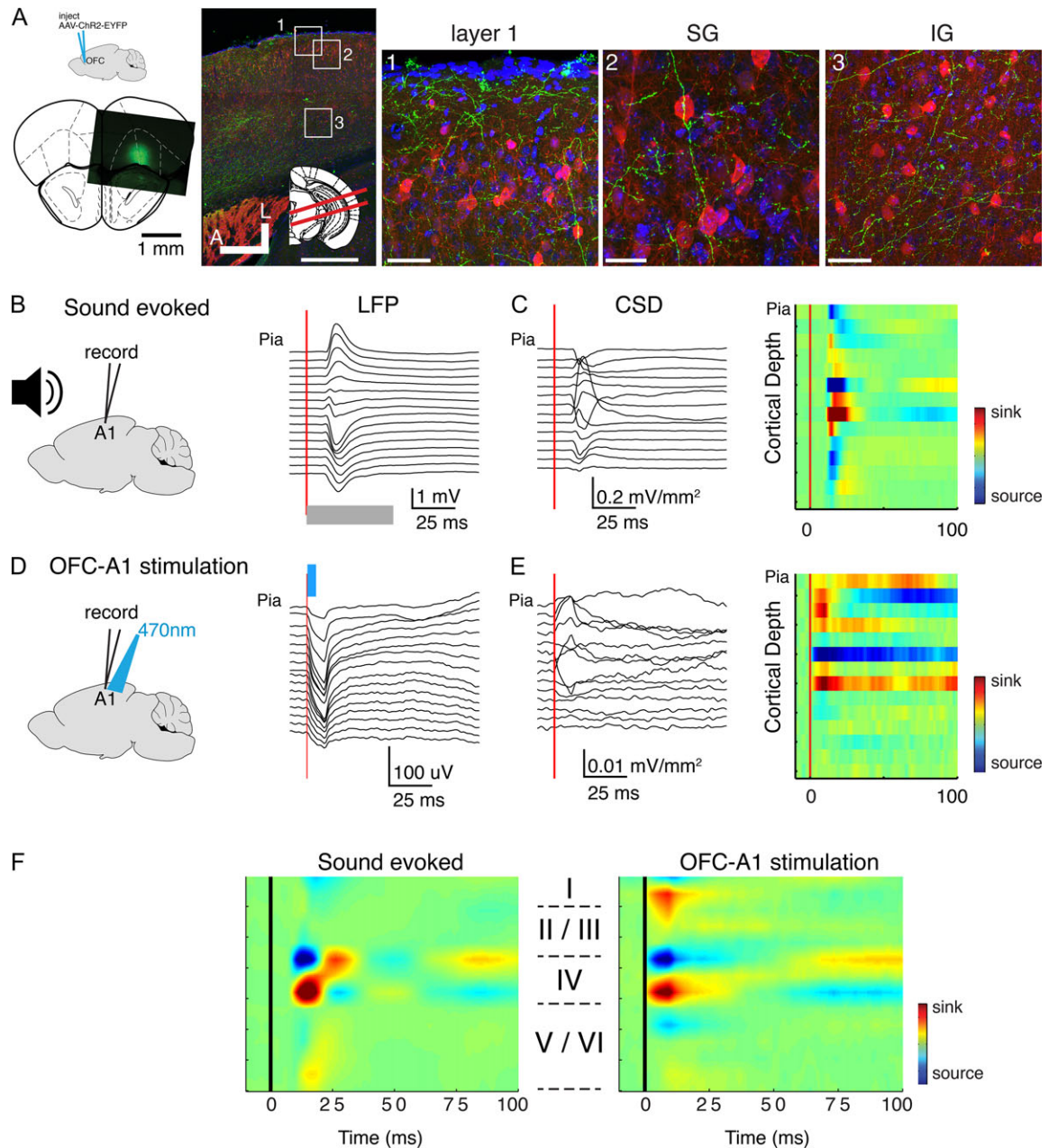


Figure 3. Optogenetic stimulation of OFC axons in vivo elicits activity in A1. (A) OFC axons are present in A1. Left: top: schematic shows that AAV-ChR2-EGFP was injected into OFC. Bottom: image indicating location of a representative injection site. Image on right shows brain slice through A1 visualizing OFC fibers in A1 (green). Inset: red lines indicate slice angle (15° from horizontal). Squares indicate regions of interest shown in 1–3. Green: labeled OFC axons in Layer 1 and upper L2/3. Blue: DAPI; red: Gad. Scale bar: 500 μm. (1) High magnification view of pial surface of A1. Scale bar: 50 μm. (2) High magnification view of L2/3 in A1. Scale bar: 25 μm. (3) High magnification view of L5/6 in A1. Scale bar: 50 μm. (B) Example sound-evoked LFPs (ERPs) recorded from linear 16 channel array. Gray bar denotes sound onset and duration. (C) Sound-evoked CSD (left) and pseudocolor representation (right) derived from voltage traces in (B). (D) Example light-evoked ERPs recorded from same location as in (A). Light (470 nm) was targeted to the A1 recording location activating OFC terminals. Blue bar denotes light onset and duration. (E) Light-evoked CSD profile (left) and pseudocolor representation (right) derived from voltage traces in (D). (F) Population averages of auditory evoked (left) and optogenetically evoked (right) CSD profiles.

target A1 neurons in many laminae. Therefore, we next investigated in vitro which neurons receive direct OFC input. To selectively activate OFC projections, we injected AAV-ChR2 into OFC and, after a survival time of several weeks, cut TC slices of A1 and performed in vitro whole-cell patch-clamp recordings from neurons in cortical layers 2/3, 4, 5, and 6 (Fig. 4A). Cells were initially patched blindly in thick (500–600 μm) slices from adult animals. We activated OFC projections by full field blue

(470 nm) light stimulation. To identify glutamatergic connections, we held cells at -70 mV and identified short-latency (<25 ms) excitatory post-synaptic current (EPSCs). In normal ACSF, a small EPSC could be evoked in approximately 50% (8/17) of cells (Fig. 4B). However, because the lack of a response in some neurons might be due to weak ChR2 expression in some axon terminals, we enhanced ChR2-evoked release by adding a low concentration of 4-AP (10–20 μM) to the bath for a subset of

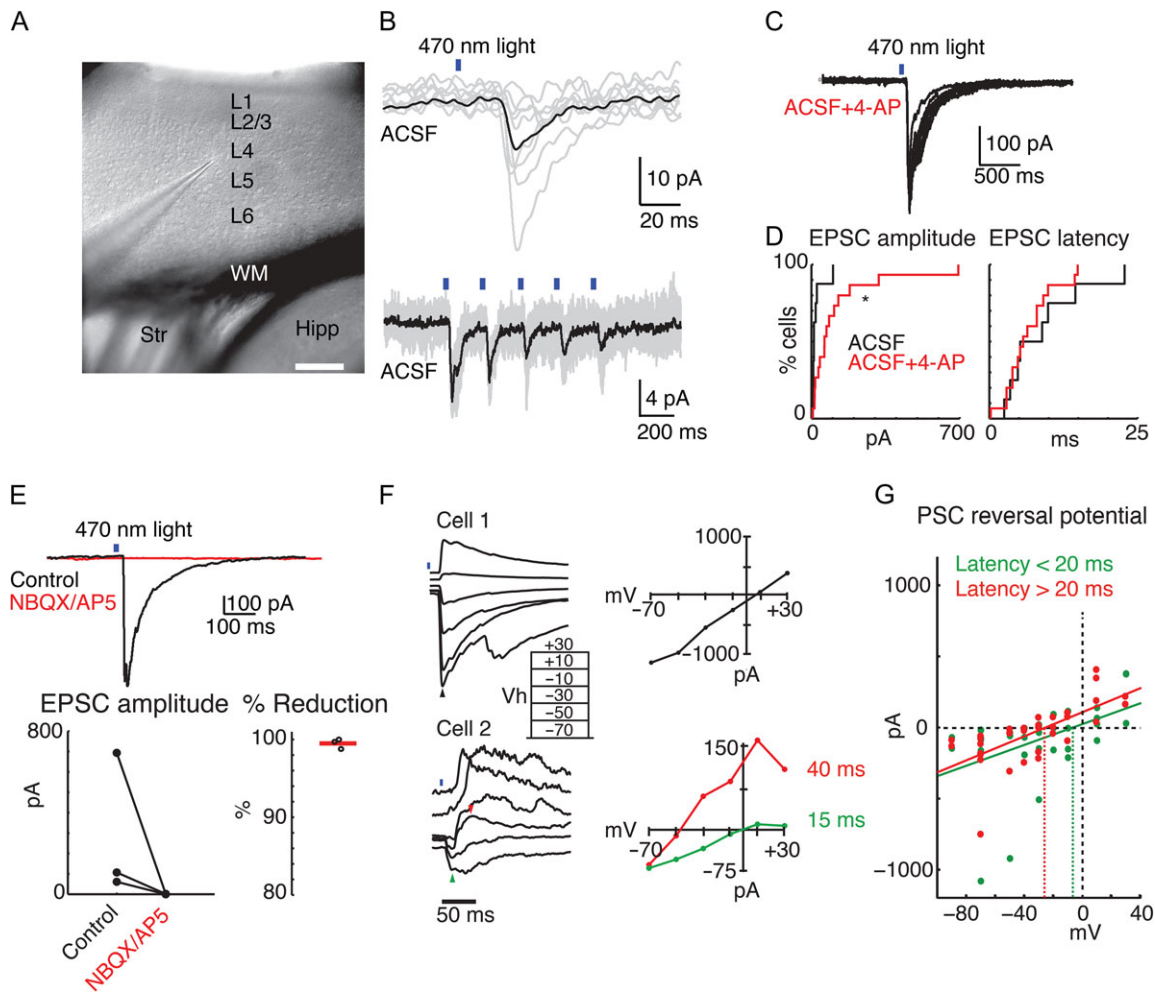


Figure 4. Optogenetic stimulation of OFC axons in vitro elicits EPSCs in A1 neurons. (A) Low-power infrared image of an A1 TC slice. A neuron is being patched in L4. Scale bar 250 μm . (B) Upper trace, example of Chr2-evoked postsynaptic current (PSC) in the cell recorded from in A. Black trace is the mean of successive stimulation trials (gray traces). Lower trace, different cells, 5 Hz light stimulation elicited synchronous train of PSCs. Recordings done in normal ACSF, at a holding potential of -70 mV. (C) Recording performed in the presence of 4-AP. (D) Cumulative distribution functions of PSC amplitude (left) and onset latency (right) recorded from cells patched blindly in 500–600 μm A1 TC slices. Cells patched in normal ACSF are in black ($N = 8$) and cells patched in ACSF + 10–20 μM 4-AP are in red ($N = 15$). 4-AP significantly increased amplitudes ($P = 0.023$) but did not change latency of PSCs ($P = 0.899$). (E) Averaged response in a single cell before (black trace) and after (red trace) application of iGluR antagonists NBQX and AP5. The response was completely blocked by the iGluR antagonists. Below the averaged trace, summary plots show the amplitude of EPSCs before and after adding iGluR antagonists (left), and the percent reduction by iGluR antagonists (right) for $n = 3$ cells. 4-AP is present. (F) Reversal potentials obtained from blindly patched A1 cells (likely pyramidal). Top recording, single PSC with a reversal potential near 0 mV indicates monosynaptic glutamatergic transmission. Bottom recording, possible disynaptic response, having a fast component reversing near 0 mV (green triangle in the trace, green line in the IV plot) and a slower component (red triangle in the trace, red line in the IV plot) reversing near -50 mV (ca. E_{Cl}). Both recordings performed in the presence of 4-AP. (G) Summary of reversal potentials of early (0–20 ms) and late (20–100 ms) components of PSCs from $n = 7$ cells. Green and red dots indicate individual current amplitudes measured during the early and late time periods, respectively. Green and red diagonal lines are best linear fit for all individual early and late responses, respectively. Green and red dashed vertical lines indicate zero current intercept and thus the reversal potential of the component. Note that the reversal potential of the late component is more negative than that of the short-latency component.

cells. Under these conditions, an EPSC could be evoked in approximately 75% (16/21) of cells (Fig. 4C). EPSC amplitudes were larger in cells recorded with 4-AP (mean \pm SEM: 24.2 ± 11.3 pA vs. 121.8 ± 45.8 pA with 4-AP, $P < 0.05$, KS-test, Fig. 3D). Response latencies, however, were unchanged by 4-AP (mean \pm SEM: 9.0 ± 2.4 ms vs. 6.7 ± 1.1 ms with 4-AP, $P > 0.8$, KS-test, Fig. 4D). Thus, it is unlikely that 4-AP is simply enhancing indirect polysynaptic activation of cells following OFC axon stimulation. Most top-down intracortical connections are glutamatergic. Indeed, light-evoked responses were blocked by adding the ionotropic glutamate receptor (iGluR) antagonists NBQX and D-AP5 ($n = 3$ cells; Fig. 4E), and no responses could be

evoked in slices pretreated with antagonists ($n = 2$ cells), confirming that the OFC-A1 projection is glutamatergic. We next sought to identify the reversal potential of the evoked postsynaptic currents (PSCs) by varying the holding potential from -70 to $+30$ mV. When measuring the reversal potential of the Chr2-evoked currents in a subset of cells (3/7), we noted that responses had longer latency components that clearly reversed nearer to the Cl^- equilibrium potential of approximately -60 mV (Fig. 4F). We therefore calculated 2 reversal potentials for each cell—one each at the peak of the response from 0 to 20 ms, and from 20 to 100 ms poststimulus. Indeed, while the earlier component reversed nearer to the expected glutamate

receptor reversal potential (0 mV), the later component reversed near -30 mV—closer to the expected GABA reversal potential (E_{Cl}) (Fig. 4F,G). These results suggest that OFC stimulation could provide diffuse, excitatory input to both pyramidal cells and interneurons in A1.

OFC Provides Excitation to Both Pyramidal Cells and Interneurons in A1

While the complexity of the reversal potentials (Fig. 4F) suggests that both pyramidal cells and interneurons are modulated by OFC input, the “blind” nature of the recordings, the slightly enhanced tissue excitability in the presence of 4-AP, and the fact that the longer latency response component (20–100 ms) reversed nearer to the Cl^- equilibrium potential than the early response, leaves open the possibility that interneurons are only activated indirectly by OFC input. Our previous work demonstrated that pairing OFC stimulation with sounds results in a specific decrease in sound-evoked gamma power (Winkowski et al. 2013). Since gamma oscillations are thought to be driven by inhibitory neurons (Buzsaki and Wang 2012), we speculated that OFC projections might directly innervate A1 inhibitory neurons. We investigated this hypothesis directly by recording from GABAergic neurons. We used mice in which most GABAergic neurons express td-Tomato by crossing a GAD2-IRES-Cre mouse (JAX) with the Ai9 reporter line (JAX). After injection of AAV-ChR2 into the OFC, we then performed whole-cell recordings in the labeled cells within layers 2/3, 4, 5, and 6 of A1 (Fig. 5A; all recordings were performed in the presence of $10 \mu M$ 4-AP). We found that nearly all recorded Gad2+ cells (16/17 cells, 94%) showed short-latency light-evoked inward currents, indicating that they received excitatory inputs from the OFC (Fig. 5A,B). We also patched several non-Gad2+ cells with pyramidal morphology in the same slices. We found that all pyramidal cells (12/12, 100%) showed light-evoked currents, which were of comparable amplitude and latency as those recorded in interneurons (Fig. 5B). We could detect no gross laminar differences in response amplitude (Fig. 5C) and latency (Fig. 5D) between pyramidal cells and interneurons. Thus, these results indicate that OFC signals diffuse throughout all layers to both excitatory and inhibitory neurons in A1, and as such could affect the balance of excitation and inhibition across the whole A1 column.

Optogenetic Activation of OFC-A1 Projection Can Cause Receptive Field Plasticity in A1

Electrical stimulation of the OFC causes receptive field plasticity in A1, which is visible as altered receptive fields of single neurons and reduced power of the sound-evoked LFP indicating desynchronization (Winkowski et al. 2013). While the OFC might influence A1 via multiple pathways, the observed OFC-induced plasticity in A1 was present even if cholinergic signaling was blocked, suggesting that indirect pathways from the OFC to A1, for example, via the cholinergic basal ganglia, were not involved (Winkowski et al. 2013). To determine whether the selective activation of the direct OFC-A1 pathway contributes to frequency-specific changes in sound-evoked responses in A1, we performed electrophysiological experiments in which we recorded A1 LFP activity before and after pairing a sound stimulus with optogenetic activation of OFC axons at the recording location in A1 ($n = 6$ animals). To sample responses over a complete cortical column in A1, we used a 16-site linear array electrode and sampled LFPs across all layers. To prevent

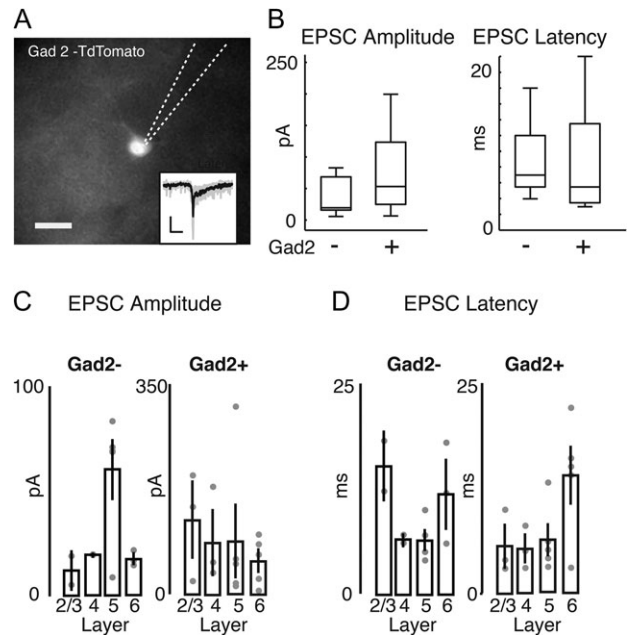


Figure 5. Short-latency EPSCs are evoked in both interneurons and pyramidal cells following optogenetic stimulation of OFC axons. (A) Fluorescence image of a Td-Tomato expressing cell in a TC slice from Gad2-Td-tomato mouse, injected with AAV-ChR2 in the left OFC. Dotted lines show the outline of the recording pipette. Scale bar $10 \mu m$. Inset trace shows that a light-evoked EPSC is from the same cell. Thus, light stimulation of OFC axons evokes EPSCs in interneurons in A1. (B) Boxplots of EPSC peak amplitude (left) and onset latency (right) of cells recorded in Gad-Td-Tomato mice that were Td-tomato+ (presumed interneurons) or Td-tomato negative with pyramidal morphology (presumed pyramidal cells). There are no significant differences between pyramidal cells and interneurons for either PSCs peak amplitude or latency ($P > 0.05$, rank-sum test; $P = 0.054$ for EPSC amplitude comparison). (C) Amplitude of EPSCs in Gad+ and Gad- neurons separated by recording lamina. Dots indicate values for individual cells, bars show mean \pm SEM. (D) Onset Latency of EPSCs in Gad+ and Gad- neurons separated by recording lamina. Dots indicate values for individual cells, bars show mean \pm SEM.

antidromic activation of other pathways originating in the OFC, we applied GABA agonists in OFC (see Methods). To determine changes in A1 LFPs, we computed sound frequency-tuning curves for each recording channel using the average of the peak-to-peak LFP amplitude across repetitions for all presented sounds before and after OFC-sound pairing episodes (Fig. 6A). In the case shown, 12-kHz (arrow) was selected as the pairing frequency (PF); other sound frequencies were used in other experiments. After OFC-sound pairing, the 12-kHz evoked LFPs were significantly suppressed (Fig. 6A,B, arrows). This frequency-specific suppression at the paired frequency was consistent across the population (Fig. 6C) and was reminiscent of the effects of electrical OFC stimulation (Winkowski et al. 2013). To account for differences in overall LFP amplitude across experiments, we computed a modulation index for each recording site [(post-pre)/(post+pre)]. We found a significant suppression of responses at the PF and no change in response for sounds one octave (above or below) away from the PF (Fig. 6D). This was not the case when we simply repeated a sound of a single frequency without activating OFC axons ($n = 4$ animals; Fig. 6C,E) indicating that the observed effect was not due to habituation but specific to activation of OFC fibers. We next compared the effect of OFC-A1 activation on activity in each lamina. The observed changes in sound-evoked responses were present with the same effect size in all laminae (Fig. 6F). Thus, our results show that activation of the

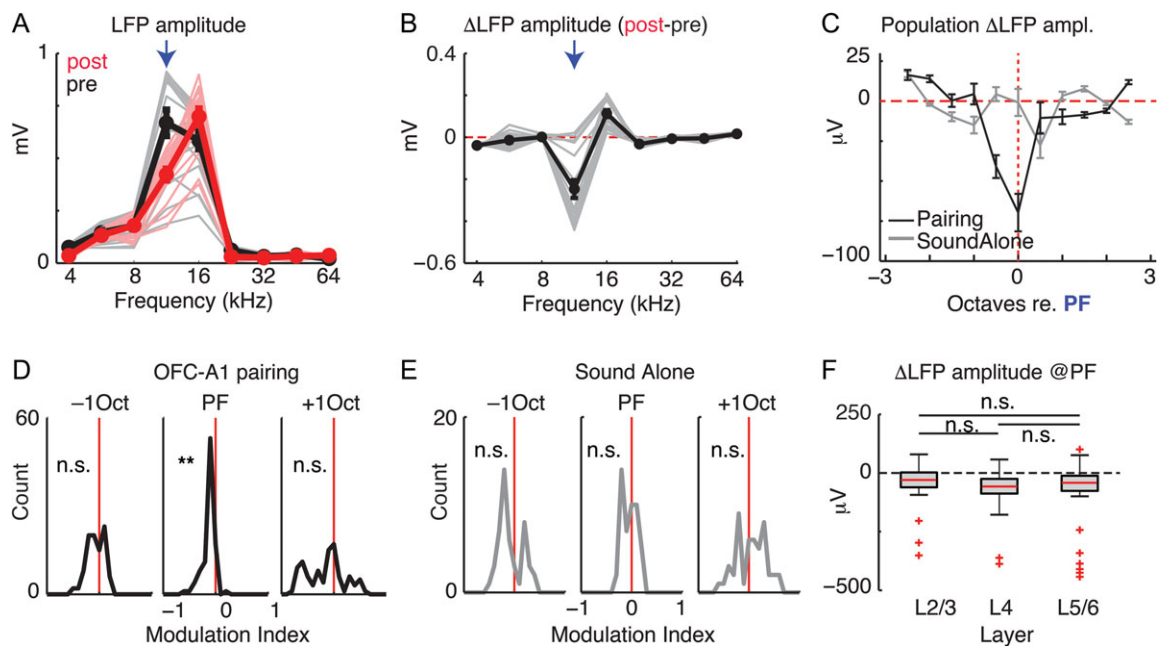


Figure 6. Pairing optogenetic stimulation of OFC axons in vivo with sounds changes sound-evoked responses in A1. (A) Sound-evoked LFP amplitude (peak-to-peak) as a function of sound frequency before (black) and after (red) pairing selective optogenetic stimulation of OFC axons with 12 kHz (arrow). Thin lines indicate responses averaged across repeats recorded on each channels before (gray, pre) and after (red, post) OFC-sound pairing episode. Thick lines are the mean responses across all channels. Error bars: SEM. (B) Difference (post-pre) in response amplitude to sounds after OFC optical pairing episode. Thin gray lines are the changes on each channel; thick black line: average across all channels. Error bars: SEM. Arrow indicates PF of 12 kHz. (C) Average changes in response amplitude (post-pre) for pairing experiments (black, filled circles) and sound alone experiments (gray, open circles) for the population ($n = 6$ animals; 96 recording channels). The frequency axis was normalized to the PF in every experiment. (D) Modulation indices for changes in response amplitude across responsive channels at the PF and ± 1 octave away. $**P < 10^{-7}$; n.s., not significant $P > 0.1$. (E) Modulation indices for changes in response amplitude across responsive channels for sound alone control; n.s., not significant $P > 0.1$. (F) Changes in response amplitude at the PF grouped by laminar position. LFP amplitudes at the PF are reduced in each lamina ($P < 0.05$). Effects were similar across all laminar groupings; n.s., not significant $P > 0.1$.

OFC-A1 projection results in specific changes in the sound-evoked activity in all layers of A1. Moreover, optical stimulation of the OFC-A1 pathway leads to changes in the A1 LFP that are similar to changes observed with electrical stimulation of OFC (Winkowski et al. 2013). Thus, the effects of electrical OFC stimulation on A1 are mostly due to direct OFC-A1 projections.

Discussion

We show that the OFC in mice responds to sound stimuli and that OFC neurons sends projections directly to A1 to form excitatory synapses on excitatory pyramidal and inhibitory interneurons across all A1 laminae. Optogenetic activation of this pathway in vivo paired with a PT alters the sound-evoked LFP activity in A1 specifically for the paired tone consistent with prior electrical OFC stimulation results (Winkowski et al. 2013). Together, these findings identify a circuit that could be important for understanding how sensory representations are dynamically adjusted to maintain stable perception of the surroundings and to adapt sensory responses to reflect changing behavioral relevance of incoming stimuli.

The existence of corticocortical connections between OFC and A1 that we observed in mice are consistent with previous anatomical investigations in most mammals ranging from rodents to primates (Petrides and Pandya 1988; Budinger et al. 2008). Here, we further show that OFC projections are broadly distributed across all A1 laminae and innervate both excitatory as well as inhibitory (Gad2 expressing) neurons. The broad laminar distribution of OFC axons in A1 would suggest that OFC axons could regulate A1 activity at many stages within a

cortical column; consistent with our in vivo electrophysiology observations. Moreover, the OFC activation of A1 interneurons would suggest the potential for this OFC projection to influence the balance of excitation and inhibition in auditory cortical networks and thereby dynamically regulate sound-evoked activity and frequency selectivity; consistent with our prior electrical OFC stimulation results (Winkowski et al. 2013).

Our results show that neurons in the OFC show robust, but fairly non-selective responses to acoustic stimuli in the OFC of the awake mouse, in the absence of any prior training to associate sound with reward. Future studies are needed to explore whether selective auditory responses in OFC develop after auditory learning. Although the mouse OFC is known to play a key role in associating sensory stimuli with reward (Schoenbaum et al. 2009; Wilson et al. 2014), the sensory inputs to OFC that have mostly been studied are visual, somatosensory, and especially those associated with food (olfactory and gustatory). To our knowledge, there have been almost no previous studies of mouse OFC responses to auditory stimuli, thus our results are the first to demonstrate the intimate association of OFC and A1 in the mouse (although there is evidence for higher order auditory cortical projections to the homologous lateral and medial OFC in the primate [Saleem et al. 2014]).

The results of the in vitro optogenetic experiments demonstrate that most A1 neurons receive direct OFC input. We did not find any obvious differences in postsynaptic response properties between pyramidal cells and interneurons, or between cortical layers in A1, although our results do not rule out subtle cell-type or laminar-specific differences in OFC-A1 connections. Given the extremely high percentage of both interneurons and

pyramidal cells which received OFC input, it is very likely that even sparse input from the OFC can drive feedforward or feedback inhibition in A1 in vivo. Finally, the Gad2+ cells from which we recorded are likely representative of the diversity of the interneuron population, yet nearly all of our recorded cells received OFC input. This suggests that OFC input to interneurons in A1 is broad and not subtype-dependent.

We showed that optogenetic activation of OFC axons in A1 when paired with a sound stimulus suppresses responses to the paired stimulus and that the magnitude of these OFC-induced changes are similar across laminae. The frequency-specific suppression of the LFP in particular in the gamma band was also observed with electrical OFC stimulation and could be due to desynchronization of the local neuronal population (Winkowski et al. 2013). Suppression of sound-evoked activity is a phenomenon that has been observed under a variety of conditions including when animals are engaged in an active listening task compared to when they are passively listening (Otazu et al. 2009), during a positive reinforcement go-nogo discrimination task (David et al. 2012), during self-generated sounds or vocalizations (Eliades and Wang 2008, 2013; Reznik et al. 2015, 2015; Behroozmand et al. 2016), or by activating axon terminals of neurons originating in the motor cortex (Nelson et al. 2013; Schneider et al. 2014). The widespread paradigms through which suppressive effects (as well as reports of enhanced responses) (Fritz et al. 2003, 2005) can be produced suggest that there are a multitude of strategies by which higher order areas and/or cognitive processes can alter spontaneous and/or sensory driven cortical activity. This holds true for our recent studies in which we applied electrical stimulation to sites in the OFC under the same conditions as the current study (Winkowski et al. 2013). Using in vivo 2-photon Ca²⁺ imaging, we found a diverse set of changes to neuronal responses after OFC electrical stimulation-sound pairing episodes that, on average, resulted in an enhancement of neural responses at or close to the paired sound frequency and improved neural discrimination of the paired sound compared with other sounds (Winkowski et al. 2013). One potential confound of electrical stimulation is that it potentially also activates indirect pathways leading from OFC to A1, for example, those via neuromodulatory and limbic areas (Cavada et al. 2000; Golmayo et al. 2003; Budinger et al. 2008). However, blocking cholinergic signaling pharmacologically did not abolish the effect electrical OFC stimulation (Winkowski et al. 2013). The similarity of our current results to the effects of electrical OFC stimulation (Winkowski et al. 2013) suggests that electrical OFC stimulation predominantly engages the OFC-A1 projections.

Here, we set out to describe, in further detail, the anatomical and functional connectivity between OFC and A1 and investigate whether direct OFC projections have any influence over A1 stimulus-driven activity. The OFC-A1 circuit that we have described possesses many features that allow it to regulate A1 sound-evoked activity. The anatomical connections are broadly distributed across laminae and form synaptic contacts with both excitatory and inhibitory neurons. Together, these features of the OFC projection make it capable of guiding changes to A1 stimulus-driven activity. Direct top-down projections to A1 are not unique to the auditory system. Prior studies have revealed a direct influence of motor cortex on primary somatosensory cortex (Veinante and Deschenes 2003; Petreanu et al. 2012) and cingulate cortex on mouse primary visual cortex (Zhang et al. 2014). Together, these results from many sensory systems show that ascending afferent information is already gated and/or shaped at the initial processing stages of the cerebral cortex in the

rodent. Therefore, descriptions of sensory cortical processing need to take into account the internal states of the animal and also the history of the animal that can both modulate incoming sensory information. Moreover, disruptions or hypofunction of the specific connection between the OFC and auditory cortex are likely to yield deficits in auditory attention and might underlie a variety of symptoms of auditory cognitive disorders.

Funding

National Institute of Deafness and Communication Disorders (NIDCD) R01DC009607 (P.O.K.); NIDCD R01DC005779 (S.A.S.); NIDCD T32 46-20 (D.N.); Office of Naval Research N00014-12-1-0855 (J.B.F.).

Notes

D.W., D.N., S.A.S., J.B.F., and P.O.K. designed research. D.W. performed tracer and virus injections, histological processing, and in vivo A1 recordings. D.N. performed in vitro recordings. K.J.D. performed in vivo OFC recordings and subsequent histochemistry and neuroanatomical localization, D.W., D.N., P.Y., K.J.D., and J.B.F. analyzed the data. We thank Yasi Etemadi and Shahzeib Syed for technical assistance with histology and immunohistochemistry. D.W., D.N., K.J.D., P.Y., J.B.F., and P.O.K. discussed the results and wrote the manuscript. *Conflict of Interest:* None declared.

References

- Behroozmand R, Oya H, Nourski KV, Kawasaki H, Larson CR, Brugge JF, Howard MA 3rd, Greenlee JD. 2016. Neural correlates of vocal production and motor control in human Heschl's gyrus. *J Neurosci.* 36:2302–2315.
- Budinger E, Laszcz A, Lison H, Scheich H, Ohl FW. 2008. Non-sensory cortical and subcortical connections of the primary auditory cortex in Mongolian gerbils: bottom-up and top-down processing of neuronal information via field AI. *Brain Res.* 1220:2–32.
- Buzsaki G, Wang XJ. 2012. Mechanisms of gamma oscillations. *Annu Rev Neurosci.* 35:203–225.
- Cavada C, Company T, Tejedor J, Cruz-Rizzolo RJ, Reinoso-Suarez F. 2000. The anatomical connections of the macaque monkey orbitofrontal cortex: a review. *Cereb Cortex.* 10:220–242.
- David SV, Fritz JB, Shamma SA. 2012. Task reward structure shapes rapid receptive field plasticity in auditory cortex. *Proc Natl Acad Sci U S A.* 109:2144–2149.
- Eliades SJ, Wang X. 2008. Neural substrates of vocalization feedback monitoring in primate auditory cortex. *Nature.* 453:1102–1106.
- Eliades SJ, Wang X. 2013. Comparison of auditory-vocal interactions across multiple types of vocalizations in marmoset auditory cortex. *J Neurophysiol.* 109:1638–1657.
- Englitz B, David SV, Sorenson MD, Shamma SA. 2013. MANTA—an open-source, high density electrophysiology recording suite for MATLAB. *Front Neural Circuits.* 7:69.
- Fritz J, Shamma S, Elhilali M, Klein D. 2003. Rapid task-related plasticity of spectrotemporal receptive fields in primary auditory cortex. *Nat Neurosci.* 6:1216–1223.
- Fritz JB, David SV, Radtke-Schuller S, Yin P, Shamma SA. 2010. Adaptive, behaviorally gated, persistent encoding of task-relevant auditory information in ferret frontal cortex. *Nat Neurosci.* 13:1011–1019.

- Fritz JB, Elhilali M, Shamma SA. 2005. Differential dynamic plasticity of A1 receptive fields during multiple spectral tasks. *J Neurosci.* 25:7623–7635.
- Golmayo L, Nunez A, Zaborszky L. 2003. Electrophysiological evidence for the existence of a posterior cortical-prefrontal-basal forebrain circuitry in modulating sensory responses in visual and somatosensory rat cortical areas. *Neuroscience.* 119:597–609.
- Mao T, Kusefoglu D, Hooks BM, Huber D, Petreanu L, Svoboda K. 2011. Long-range neuronal circuits underlying the interaction between sensory and motor cortex. *Neuron.* 72:111–123.
- Mitzdorf U, Singer W. 1978. Prominent excitatory pathways in the cat visual cortex (A 17 and A 18): a current source density analysis of electrically evoked potentials. *Exp Brain Res.* 33:371–394.
- Nelson A, Schneider DM, Takato J, Sakurai K, Wang F, Mooney R. 2013. A circuit for motor cortical modulation of auditory cortical activity. *J Neurosci.* 33:14342–14353.
- Otazu GH, Tai LH, Yang Y, Zador AM. 2009. Engaging in an auditory task suppresses responses in auditory cortex. *Nat Neurosci.* 12:646–654.
- Paxinos G, Franklin K. 2013. The mouse. In: *Brain in stereotaxic coordinates.* New York: Academic Press. p. 60.
- Petreanu L, Gutnisky DA, Huber D, Xu NL, O'Connor DH, Tian L, Looger L, Svoboda K. 2012. Activity in motor-sensory projections reveals distributed coding in somatosensation. *Nature.* 489:299–303.
- Petrides M, Pandya DN. 1988. Association fiber pathways to the frontal cortex from the superior temporal region in the rhesus monkey. *J Comp Neurol.* 273:52–66.
- Reznik D, Henkin Y, Levy O, Mukamel R. 2015. Perceived loudness of self-generated sounds is differentially modified by expected sound intensity. *PLoS one.* 10:e0127651.
- Reznik D, Ossmy O, Mukamel R. 2015. Enhanced auditory evoked activity to self-generated sounds is mediated by primary and supplementary motor cortices. *J Neurosci.* 35:2173–2180.
- Saleem KS, Miller B, Price JL. 2014. Subdivisions and connective networks of the lateral prefrontal cortex in the macaque monkey. *J Comp Neurol.* 522:1641–1690.
- Schneider DM, Nelson A, Mooney R. 2014. A synaptic and circuit basis for corollary discharge in the auditory cortex. *Nature.* 513:189–194.
- Schoenbaum G, Roesch MR, Stalnaker TA, Takahashi YK. 2009. A new perspective on the role of the orbitofrontal cortex in adaptive behaviour. *Nat Rev Neurosci.* 10:885–892.
- Suter BA, O'Connor T, Iyer V, Petreanu LT, Hooks BM, Kiritani T, Svoboda K, Shepherd GM. 2010. Ephus: multipurpose data acquisition software for neuroscience experiments. *Front Neural Circuits.* 4:100.
- Veinante P, Deschenes M. 2003. Single-cell study of motor cortex projections to the barrel field in rats. *J Comp Neurol.* 464:98–103.
- Whitton JP, Hancock KE, Polley DB. 2014. Immersive audio-motor game play enhances neural and perceptual salience of weak signals in noise. *Proc Natl Acad Sci U S A.* 111:E2606–E2615.
- Wilson RC, Takahashi YK, Schoenbaum G, Niv Y. 2014. Orbitofrontal cortex as a cognitive map of task space. *Neuron.* 81:267–279.
- Winkowski DE, Bandyopadhyay S, Shamma SA, Kanold PO. 2013. Frontal cortex activation causes rapid plasticity of auditory cortical processing. *J Neurosci.* 33:18134–18148.
- Yang WW, Zhou XM, Zhang JP, Sun XD. 2007. Modulation of frequency receptive field plasticity in rat auditory cortical neurons by electrical stimulation of medial prefrontal cortex. *Sheng Li Xue Bao.* 59:784–790.
- Zhang S, Xu M, Chang WC, Ma C, Hoang Do JP, Jeong D, Lei T, Fan JL, Dan Y. 2016. Organization of long-range inputs and outputs of frontal cortex for top-down control. *Nat Neurosci.*
- Zhang S, Xu M, Kamigaki T, Hoang Do JP, Chang WC, Jenvay S, Miyamichi K, Luo L, Dan Y. 2014. Selective attention. Long-range and local circuits for top-down modulation of visual cortex processing. *Science.* 345:660–665.
- Zhao C, Kao JP, Kanold PO. 2009. Functional excitatory microcircuits in neonatal cortex connect thalamus and layer 4. *J Neurosci.* 29:15479–15488.